Applied Catalysis B: Environmental 241 (2019) 104–112

Contents lists available at ScienceDirect

Applied Catalysis B: Environmental

journal homepage: www.elsevier.com/locate/apcatb

In-situ growth of Co_3O_4 nanowire-assembled clusters on nickel foam for aqueous rechargeable Zn-Co_3O_4 and Zn-air batteries

Peng Tan[a,b], Bin Chen[b], Haoran Xu[b], Weizi Cai[b], Wei He[b], Meng Ni[b,c,*]

[a] Department of Thermal Science and Energy Engineering, University of Science and Technology of China, Hefei 230026, China
[b] Department of Building and Real Estate, The Hong Kong Polytechnic University, Hung Hom, Kowloon, Hong Kong, China
[c] Environmental Energy Research Group, Research Institute for Sustainable Urban Development (RISUD), The Hong Kong Polytechnic University, Hung Hom, Kowloon, Hong Kong, China

ARTICLE INFO

Keywords:
Cobalt oxide
Nanowire-assembled clusters
Binder-free
Alkaline solution
Zinc battery

ABSTRACT

With the urgent requirements for advanced energy storage systems, rechargeable Zn-based batteries attract research interest due to the remarkable theoretical capacity, low cost, and environmental benignity. Hence, developing effective battery materials are in great need. In this work, an electrode composed of Co_3O_4 nanowire-assembled clusters is developed. The porous Co_3O_4 nanowires are directly coupled to the underlying nickel foam to form clusters, avoiding the use of additional binders and conductive carbons. This hierarchical structure not only provides large active surfaces and facilitates species transport, but also favors the structural stability. In an alkaline solution, this electrode exhibits high activity toward both oxygen reduction and evolution reactions and large specific capacitance, indicating the excellent electrochemical performance. A Zn-Co_3O_4 battery using this electrode delivers an energy density up to 239 Wh kg^{-1} on the basis of the Co_3O_4 loading and the theoretical capacity of zinc, and the capacity retention reaches 84.1% after 1000 cycles. Moreover, a hybrid Zn-Co_3O_4/air battery fitted with the present electrode exhibits a high capacity of 771 mAh g_{Zn}^{-1} and excellent cycling stability for over 1000 cycles (over 333 h) at 10 mA cm^{-2} with a fixed capacity of 1.67 mA cm^{-2} while maintaining the energy efficiency of ~70%. The results show that the nickel foam coated with Co_3O_4 nanowire-assembled clusters is a promising electrode for high-performance rechargeable Zn-based batteries with high energy density, energy efficiency, and cycling stability.

1. Introduction

The advancement in electric vehicles and portable electronic devices requires high-energy-density energy storage systems [1,2]. Lithium-ion batteries, owing to the remarkable energy density, excellent cycle life, and high energy efficiency [3], have attracted great attention and been rapidly developed [4]. However, the high price of raw materials used in batteries limits the large-scale applications [5]. Moreover, the safety issues originated from the highly flammable non-aqueous electrolytes and lithium-based electrodes have also caused public concerns [6]. To this end, searching for alternative battery systems with excellent electrochemical performance, low price, and high safety is in urgent demand [7].

Zinc-based batteries, which use aqueous electrolytes, have offered good alternatives to lithium-ion batteries. They have striking features for various applications, including high theoretical capacity (820 mAh g_{Zn}^{-1}), low price, and intrinsically safe [8]. In terms of the structure, zinc batteries can be classified into two types. One is a closed system, such as Zn-Mn [9,10], Zn-Ni [11,12], and Zn-Ag batteries [13–15]. In this type of batteries, the discharge and charge mechanisms are the oxidation and reduction of zinc on the negative electrode and the other redox couple (e.g., Ni^{2+}/Ni^{3+}) on the positive electrode [16]. Hence, the positive electrode materials should have high theoretical capacities, low redox potentials, and high stability to achieve good performance [17]. The other type is a half-open system, namely Zn-air batteries, in which the positive electrode is exposed to the air [18,19]. During discharge, the oxygen reduction reaction (ORR) occurs on the positive electrode, and the zinc oxidation occurs on the negative electrode; while during charge, the reactions are reversed, including the oxygen evolution reaction (OER) that releases oxygen into the air and the reduction of zinc ions to form metallic zinc [20]. Since oxygen is directly absorbed from the air and neither the mass nor the volume of the battery is occupied, the energy density is thus remarkably improved [21]. However, the discharge and charge voltage gaps are usually large

* Corresponding author at: Department of Building and Real Estate, The Hong Kong Polytechnic University, Hung Hom, Kowloon, Hong Kong, China.
E-mail address: meng.ni@polyu.edu.hk (M. Ni).

https://doi.org/10.1016/j.apcatb.2018.09.017
Received 11 July 2018; Received in revised form 31 August 2018; Accepted 8 September 2018
Available online 08 September 2018
0926-3373/ © 2018 Elsevier B.V. All rights reserved.

due to the sluggish reaction kinetics, which causes a waste of energy in charge and poor cycling stability [22]. Thus, developing effective catalyst materials with high ORR and OER activity and optimizing the positive electrode structure to facilitate oxygen transport are crucial [23–27].

Research interests have focused on Co_3O_4 as the positive electrode material for a long time owing to its high activity for oxygen electrocatalysis and remarkable theoretical capacity up to 446 mA h g^{-1} [28]. The applications of various Co_3O_4-based materials in rechargeable zinc batteries have been widely reported. For example, Chen et al. introduced Co_3O_4 nanocrystal-decorated N-doped carbon nanotubes in Zn-air batteries as an effective catalyst material and achieved low discharge-charge overpotential and a cycle life of over 100 h at 20 mA cm^{-2} [29]. Zong et al. reported an integrated air electrode composed of Co_3O_4 nanoparticle-decorated carbon nanofiber mat, which enabled a Zn-air battery with a low voltage gap of only ~0.85 V for 55 cycles at 20 mA cm^{-2} [30]. Using the Ni foam electrode covered by electrodeposited ultrathin porous Co_3O_4 nanosheets, Wang et al. developed a Zn-Co_3O_4 battery that achieved a high discharge voltage of 1.78 V, an energy density up to 241 W h kg^{-1}, and excellent cycling stability with the capacity retention of 80% after 2000 cycles [28]. In our previous work, we fabricated an electrode by growing Co_3O_4 nanosheets on carbon cloth surfaces and made a battery that combined the electrochemical reactions of Zn-Co_3O_4 and Zn-air batteries using Co_3O_4 as both reactant and electrocatalyst. The hybrid battery exhibited a high discharge voltage of 1.85 V, a remarkable capacity of 792 mAh g_{Zn}^{-1}, an excellent stability with the energy efficiency of higher than 70% for over 200 cycles (100 h), and high-rate capabilities [31]. However, the limited utilization ratio of Co_3O_4 resulted in a low discharge capacity of the Zn-Co_3O_4 reaction, and the poor activity toward oxygen electrocatalysis led to a low power density and low discharge voltage of the Zn-air reaction. Therefore, the positive electrode materials for high-performance rechargeable zinc batteries should be further explored.

In this work, we developed an electrode composed of Co_3O_4 nanowire-assembled clusters on nickel foam using a hydrothermal approach and a calcination process in the following. The characterization reveals that porous Co_3O_4 nanowires are directly grown on the nickel foam, greatly reducing the resistance in the interface and enhancing the electrical conductivity. Besides, the porous nano architecture offers large surface areas and pore volumes, which are beneficial for electrochemical reactions and species transport. Moreover, the assembled clusters are favorable for the structural stability. These features are essential for the high activity toward both ORR and OER and the large specific capacitance. The electrochemical performance of the present electrode was first evaluated in a three-electrode system, and then demonstrated in different types of rechargeable batteries. For a closed Zn-Co_3O_4 battery system, the discharge capacity, rate capability, and cycling stability were investigated. For a half-open Zn-air battery system, the power density, gravimetric capacity, as well as pulse discharge-charge stability were tested.

2. Experimental

2.1. Fabrication of Co_3O_4 nanowire-assembled clusters on nickel foam (Co_3O_4/Ni foam)

The Co_3O_4/Ni foam was fabricated by a modified hydrothermal reaction as previously reported [32]. Briefly, 2 mmol of Co $(NO_3)_2{\cdot}6H_2O$, 8 mmol of NH_4F, and 10 mmol of $CO(NH_2)_2$ were dissolved into 40 mL of distilled water to form a homogeneous solution. A piece of nickel foam was first put in a 3.0 M HCl solution and ultrasonic cleaned for 10 min to remove the possible oxide layer, then washed with distilled water and acetone, and dried thoroughly before use. The pre-treated nickel foam was put in the prepared aqueous solution, and transferred into a Teflon-lined stainless-steel autoclave. After maintained at 120 °C for 9 h and cooled down naturally to room temperature, the precursor-decorated nickel foam was taken out, rinsed with distilled water, and dried thoroughly in the air. Eventually, it was calcined at 250 °C in air for 3 h with a heating rate of 1 °C min^{-1} to convert the precursor to Co_3O_4. The loading of Co_3O_4 was calculated from the weight difference between the pristine nickel foam and the final one, which was 3.9 mg cm^{-2}.

2.2. Material characterization

The morphologies of Co_3O_4/Ni foam were observed by a scanning electron microscope (SEM, VEGA3 TESCAN) under an acceleration voltage of 20 kV, and the nanostructures were characterized by a transmission electron microscope (TEM, JEOL 2100 F) with a LaB_6 filament at 200 kV. X-ray diffraction (XRD, Rigaku Smartlab) with a Cu-Kα source operating at 45 keV was used to analyze the compositions of the synthesized materials. The X-ray photoelectron spectroscopy (XPS) data were collected by a Physical Electronics PHI 5600 multi-technique system using Al monochromatic X-ray at a power of 350 W. To measure the geometrical properties of Co_3O_4 nanowires, they were first scratched off from the Ni foam. The nitrogen adsorption-desorption isotherm of Co_3O_4 nanowires was measured by ASAP 2020 Automatic Micropore and Chemisorption Physisorption Analyzer, and the specific surface area and pore size were calculated using the Brunaure-Emmert-Teller (BET) and Barrett-Joyner-Halenda (BJH) methods, respectively.

2.3. Electrochemical measurements

A standard three-electrode system was first used to evaluate the electrochemical performance, which contains the working electrode of Co_3O_4/Ni foam, a Hg/HgO reference electrode, and a platinum wire counter electrode. To collect the current from the working electrode, the Co_3O_4/Ni foam was attached to the glassy carbon electrode using a polytetrafluoroethylene (PTFE) sleeve (Fig. S1). An alkaline solution of 0.1 M KOH was used as the electrolyte. The rotating disc electrode (RDE) voltammetry was conducted using a potentiostat (Solartron SI 1287), and the rotation speed was adjusted by a controller (Pine Instrument Co.). To measure the ORR performance, pure gaseous oxygen was purged to saturate the alkaline solution. Linear sweep voltammetry (LSV) was conducted at a rotation speed of 1600 rpm and a scan rate of 5 mV s^{-1}, and the potential ranges were 0.2 to −0.6 V (vs. Hg/HgO) for the ORR and 0.2 to 0.8 V (vs. Hg/HgO) for the OER, respectively. To measure the ORR stability, a constant potential of −0.266 V (vs. Hg/HgO) was maintained to record the current change. To measure the OER stability, the current density was maintained constantly at 40 mA cm^{-2} to record the potential change. The cycle voltammetry (CV) tests for the Co_3O_4/Ni foam electrode were conducted in the potential range of 0.2–0.7 V (vs. Hg/HgO) using the scan rates from 1 to 10 mV s^{-1}. The specific capacitance value (C) was determined using the equation [33]:

$$C = \frac{1}{msA\Delta V}\int I(V)\mathrm{d}V \quad (1)$$

where m is the loading of Co_3O_4 nanowires (mg cm^{-2}), s is the scan rate (mV s^{-1}), ΔV is the potential range (V), and $I(V)$ is the corresponding current density (mA cm^{-2}). To accurately determine the number of electrons transferred during the ORR, Co_3O_4 nanowires were scratched off from the Ni foam (4 mg), and then mixed with 2 mg of conductive carbon and 40 μL of Nafion solution (5 wt%) into 360 μL isopropanol under sonication for 30 min. After that, 4 μL of the catalyst ink was dripped onto the glassy carbon surface and dried thoroughly, and thus the loading of Co_3O_4 was 0.2 mg cm^{-2}. The ORR polarization curves were measured using different rotation speeds from 400 to 2500 rpm, and the number of electrons transferred (n) was obtained using the Koutecky-Levich equation:

$$j^{-1} = j_k^{-1} + \left(0.2nFD_{O_2}^{2/3}\nu^{-1/6}C_{O_2}\omega^{1/2}\right)^{-1} \quad (2)$$

where j and j_k are the measured and diffusion-limiting current densities, respectively, ω is the angular velocity (rpm). The values of Faraday constant (F), diffusion coefficient of O_2 (D_{O_2}), kinematic viscosity (ν), bulk concentration of O_2 (C_{O_2}) are 96,485 C mol^{-1}, 1.86×10^{-5} cm^2 s^{-1}, 1.01×10^{-2} cm^2 s^{-1}, and 1.21×10^{-6} mol cm^{-3}, respectively. In the following results, a reversible hydrogen electrode (RHE) scale was used through calibration:

$$E_{RHE} = E_{Hg/HgO} + 0.059pH + 0.098 \quad (3)$$

2.4. Fabrication and evaluation of Zn batteries

A Zn-Co_3O_4 battery was assembled using the as-prepared Co_3O_4/Ni foam and a Zn foil as the positive and negative electrodes, respectively, and an alkaline solution composed of 6 M KOH and 0.1 M zinc acetate as the electrolyte. The rate performance was tested using different current densities from 1 to 7.5 A g^{-1} based on the loading of Co_3O_4 within the voltage range of 1.3–1.95 V. For the cycling stability test, the voltage ranges were 1.3–1.93 V and 1.3–1.95 V at 1 and 5 A g^{-1}, respectively.

For the application in Zn-air batteries, the Co_3O_4/Ni foam was first soaked in 10 wt % PTFE and then dried to form a hydrophobic surface, which is beneficial for the gaseous oxygen transport. A Zn-air battery was assembled with the PTFE-treated Co_3O_4/Ni foam as the air electrode, which was attached to a carbon paper gas diffusion layer. The metal electrode was a Zn foil, and the electrolyte was composed of 6 M KOH and 0.1 M zinc acetate. The battery voltage at the current step of 1 mA s^{-1} was recorded to get the polarization curves. To evaluate the discharge performance, the voltage change was measured at a fixed current density, and the specific capacity (mAh g_{Zn}^{-1}) was calculated based the consumed Zn when the voltage dropped down to 0 V. The discharge-charge cycling stability was measured with a fixed capacity for each state.

3. Results and discussion

3.1. Characterization of Co_3O_4/Ni foam

Fig. 1a displays the morphology of the prepared Co_3O_4/Ni foam. Compared with the pristine Ni foam (Fig. S2), the smooth surface was covered by clusters uniformly. From the high-magnification SEM image in Fig. 1b, the clusters are assembled by nanowires with the average length of 5.7 μm (Fig. S3). The TEM image of one single nanowire is presented in Fig. 1c, which is composed of nanoparticles with pores formed due to the release of water molecules and the shrinkage of volume in the calcination process [34]. This porous structure can enlarger the surface area and improve the electrolyte-electrode interfacial interaction [35]. The lattice fringes of the nanocrystals are further illustrated in the high-resolution TEM image (Fig. 1c inset), and the interplanar spacings of 0.47 nm and 0.28 nm correspond to the (111) and (220) planes of crystalline Co_3O_4, respectively. To further confirm the formation of Co_3O_4, the XRD pattern of Co_3O_4/Ni foam from 10° to 90° is shown in Fig. 1d. Besides three diffraction peaks of the nickel substrate, the other peaks are almost perfectly assigned to spinel Co_3O_4 (JCPDS #42-1467). Fig. 1e shows the Co 2p electron region of the XPS spectra. The peaks located at 781.3 eV and 796.4 eV are attributable to Co^{2+}, and the peaks at 794.9 eV and 779.7 eV are indexed to Co^{3+} [36]. Fig. 1f shows the nitrogen isotherm profile of the Co_3O_4 nanowires, from which a type H1 hysteresis loop was observed, indicating the existence of mesoporous structure (Fig. 1f inset) [36]. This result agrees well with the observation from the TEM image. The specific surface area is measured to be 76.6 m^2 g^{-1}, and the pore volume is estimated to be 0.218 cm^3 g^{-1}. Hence, the characterization results indicate that Co_3O_4 nanowire-assembled clusters are in-situ grown on nickel foam without binders, enhancing the electrical property [37]. In addition, the mesoporous structure of Co_3O_4 nanowires provides a large specific surface area and shortens the species diffusion distances [38]. Moreover, the nanowire-assembled clusters increase the structural stability. These features are favorable for the improvements of electrochemical performance.

3.2. Electrochemical properties

Fig. 2 shows the ORR and OER activity of Co_3O_4/Ni foam in 0.1 M KOH solution. During the ORR process (Fig. 2a), at the potential of 0.3 V (vs. RHE), a limiting current density of -25.8 mA cm^{-2} is exhibited. The high value may come from the large mass loading of Co_3O_4 on the electrode. To more accurately measure the ORR activity, the Co_3O_4 nanowires were scratched from the nickel form to make a standard working electrode (0.2 mg cm^{-2}). As shown in Fig. S4, at the rotating speed of 1600 rpm and the potential of 0.3 V (vs. RHE), the current density reaches -4.97 mA cm^{-2}. In addition, the number of electrons transferred is measured to be around 4, indicating the four-electron process occurs on the Co_3O_4 electrode. When maintained at the potential of 0.3 V (vs. RHE) for 20 h, as shown in Fig. 2c, 82.6% of its initial current can be preserved, demonstrating the high ORR stability. In the OER region (Fig. 2b), a high current density of 40 mA cm^{-2} is obtained at the potential of 1.58 V (vs. RHE). Moreover, after maintaining at this current density for 20 h, the overpotential increases only 0.067 V (Fig. 2d), showing the high OER stability.

It is noting that in Fig. 2b a peak appears prior to the OER process. To further investigate the redox behavior of Co_3O_4, the CV curves were tested at different scan rates. From Fig. 3a, it is clear to observe that the CV curves show non-rectangular shapes, revealing the reversible redox reactions. The anodic and cathodic peaks indicate the oxidation and reduction in the electrochemical processes, respectively. Previous research has indicated that in alkaline solutions, Co_3O_4 can undergo electrochemical charge-transfer reactions of $Co^{2+} \leftrightarrow Co^{3+} \leftrightarrow Co^{4+}$ with three redox couples of $Co_3O_4/Co(OH)_2$, $Co(OH)_2$/CoOOH, and CoOOH/CoO_2 [39,40]:

$$3Co(OH)_2 + 2OH^- \leftrightarrow Co_3O_4 + 4H_2O + 2e^- \quad (I)$$

$$Co_3O_4 + OH^- + H_2O \rightleftharpoons 3CoOOH + e^- \quad (II)$$

$$CoOOH + OH^- \rightleftharpoons CoO_2 + H_2O + e^- \quad (III)$$

While in our case, the peaks that correspond to each redox couple are not evident, in which only one pair of redox peaks situated at 1.373/1.263 V (vs. RHE) can be clearly observed. The similar phenomenon has also been witnessed in the mesoporous layered hexagonal Co_3O_4 nanoparticles [41]. This might be caused by the surface condition of Co_3O_4 and/or the different alkaline concentrations [42], resulting in the overlap of redox peaks [28,43]. With an increase of the scan rate, the corresponding current density increases, and the anodic and cathodic peaks shift towards the positive and negative potential, respectively. While the shapes of CV curves are well maintained, demonstrating a good rate capability. Previous investigations have indicated that the supercapacitive properties allow to work at a higher voltage, providing a high power density and energy density [44]. The capacitance value as a function of scan rate was calculated using Eq. 1, and the results are shown in Fig. 3b. At a low scan rate of 1 mV s^{-1}, the electrolyte ions can diffuse to almost all the effective surfaces of the electrode, resulting in a high capacitance value of 1128 F g^{-1}. With an increase of the scan rate, owing to the inadequate time, the effective interaction between the electrolyte ions and the electrode is reduced, which leads to the decreased capacitance value. For the Co_3O_4/Ni foam, even the scan rate increases to a high value of 10 mV s^{-1}, the capacitance can still reach 954 F g^{-1}, demonstrating an excellent capacitance retention ratio (84.5%). This enhanced performance may come from the high surface area and the heterogeneous porous structure of the electrode, which offer accessible active sites for the intercalation of electrolyte ions [41]. The high capacitance retention indicates that the Co_3O_4/Ni foam electrode has the ability to deliver high discharge

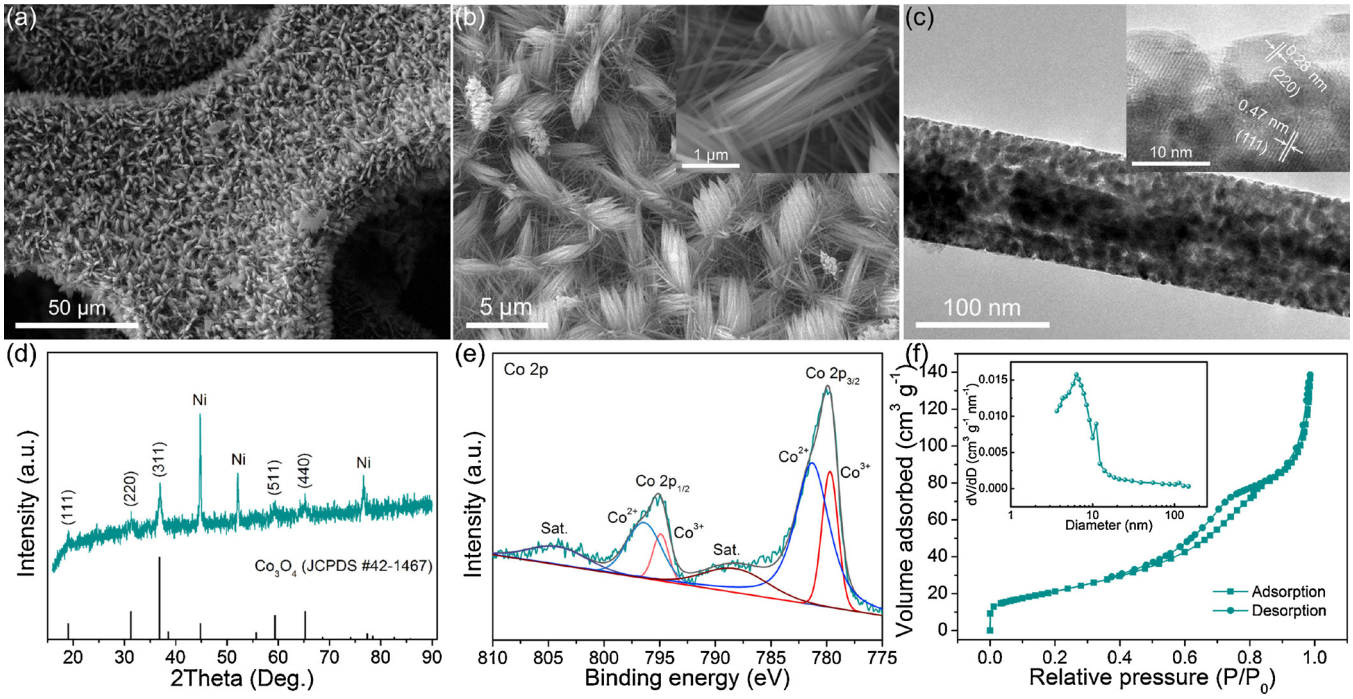

Fig. 1. Characterization of Co_3O_4 nanowire-assembled clusters on nickel foam (Co_3O_4/Ni foam). (a–b) SEM images, the inset shows the nanowires are assembled to form clusters. (c) TEM image of one nanowire, the inset shows the high-magnification TEM image. (d) XRD pattern. (e) High-resolution Co 2p XPS spectrum. (f) Nitrogen adsorption-desorption isotherm, and the inset shows the pore size distribution.

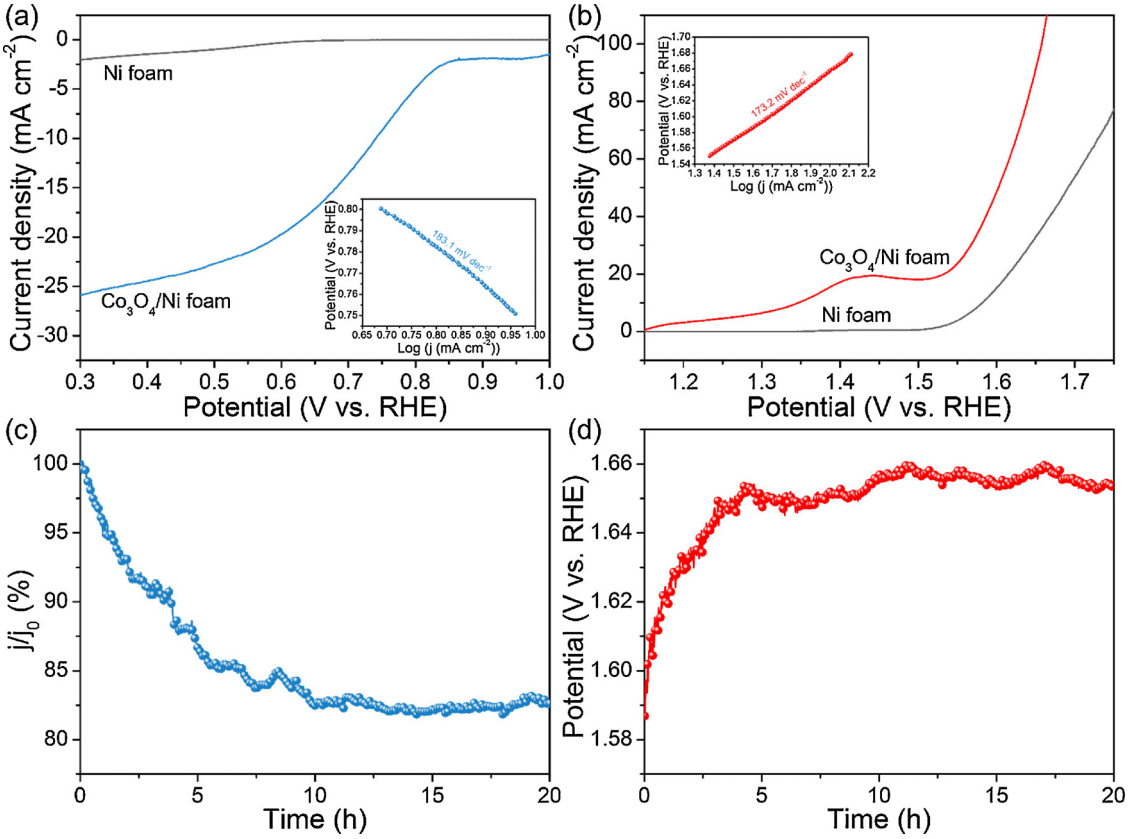

Fig. 2. Electrochemical activities of the Co_3O_4/Ni foam for oxygen reactions in 0.1 M KOH solution. LSV curves of (a) ORR and (b) OER at a scan rate of 5 mV s^{-1}, the inset shows the Tafel plots. (c) ORR chronoamperometric response a constant potential of 0.30 V (vs. RHE). (d) OER chronopotentiometric response at a constant current density of 40 mA cm^{-2}.

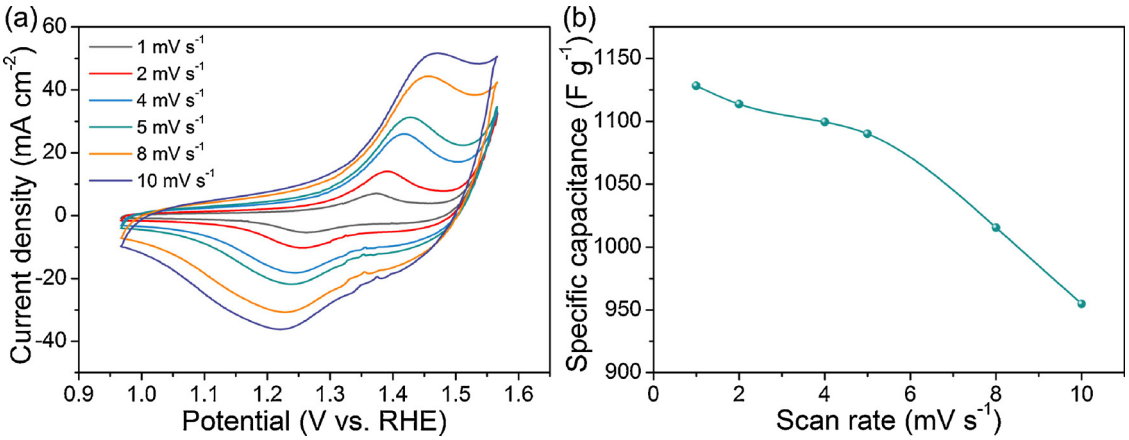

Fig. 3. (a) CV curves of Co_3O_4/Ni foam electrode in 0.1 M KOH aqueous electrolyte at various scan rates and (b) The corresponding specific capacitance.

capacities at large current densities, which is essential for the rate performance of Zn-Co_3O_4 batteries. Moreover, the supercapacitive nature of Co_3O_4/Ni foam and its high ORR and OER activity enables the hybrid Zn-Co_3O_4/air battery to operate at a higher working voltage and energy efficiency than conventional Zn-air batteries.

3.3. Performance of the Zn-Co_3O_4 battery

A home-made Zn-Co_3O_4 battery was built to evaluate the performance of the Co_3O_4/Ni foam electrode. Fig. 4a shows the voltage curves in the voltage range of 1.30 to 1.95 V. During charge, the voltage increase demonstrates the oxidation of Co_3O_4, which is proved by XRD results in Fig. S5 [45,46]. During discharge, one voltage plateau at around 1.7 V is demonstrated, consistent with the CV results. Based on the loading of Co_3O_4, the discharge capacity of the battery is 173.6 mA h g^{-1} at 1 A g^{-1}, larger than the reported battery based on Co_3O_4 nanosheets (~160 mA h g^{-1}) [28]. Owing to the excessive mass loading of zinc, on the basis of the Co_3O_4 loading and the theoretical capacity of zinc (820 mAh g^{-1}), the energy density of the battery is calculated to be 239 Wh kg^{-1}, demonstrating the high energy density feature among aqueous electrolyte-based batteries [47]. When the current density increases from 1, 2.5, 5 to 7.5 A g^{-1}, as shown in Fig. 4b, the capacity decreases from 173.6, 142.4, 95.8 to 59.0 mA h g^{-1}, respectively. In comparison, the reported Zn-Co_3O_4 battery with a Zn plate and Co_3O_4 nanosheets electrode only exhibited a capacity of ~70 mA h g^{-1} when the current density increases to 5 A g^{-1}. Hence, the Co_3O_4/Ni foam electrode enables better rate performance, consistent with the supercapacitive properties.

To evaluate the cycling stability of the battery, a small current density of 1 A g^{-1} was first applied. From the initial voltage curves in Fig. 4a, a charge voltage plateau starting from 1.93 V is observed, indicating that the oxygen evolution may occur. To this end, we adjusted the cut-off voltage to 1.93 V in the subsequent cycling test (Fig. 4c), resulting in the initial coulombic efficiency of 99% (Fig. 4d). With an increase of the cycle number, the charge capacity almost remains; however, the discharge capacity gradually decreases. This result suggests that the parasitic oxygen evolution may still occur during the charge process, which leads to a waste of energy input. After 1000 full cycles, the battery can still work, and presents the capacity retention and the coulombic efficiency of 84.1% and 86%, respectively. In comparison, the reported Zn-Co_3O_4 battery with a Zn plate and Co_3O_4 nanosheets electrode showed a capacity decay of 20% after 900 cycles [28]. Moreover, we cycled the battery using a high current density of 5 A g^{-1}. Due to the increased polarization, a charge voltage plateau is not witnessed even at the cut-off voltage of 1.95 V, suggesting that the charge process may be the sole oxidation of Co_3O_4. Consequently, an equivalent discharge capacity is delivered, leading to the coloumbic efficiency of almost 100%. With an increase of the cycle number, the charge capacity gradually decreases (Fig. 4e), and the discharge capacity decreases accordingly, giving the higher coulombic efficiency of around 100% throughout 1000 cycles, and the capacity retention can still reach 66.6% (Fig. 4f). Thus, the Zn-Co_3O_4 battery with this Co_3O_4/Ni foam electrode demonstrates high discharge capacity, rate capability, and cycling stability, which are remarkable among reported Zn-based rechargeable batteries (Table S1) [12,48–51]. To identify the reason for the capacity fading during cycling, the Co_3O_4/Ni foam electrode after cycles was further examined, from which both the morphology and the crystal structure maintain the same (Fig. S6). Previous research has also indicated that Co_3O_4 is very stable in alkaline solutions, which presented no capacitance decay after 2000 full cycles for supercapacitors [52]. Hence, in addition to the parasitic oxygen evolution reaction, the Zn electrode is thought to be responsible for the capacity fading due to the formation of dendrite and passivation layers (e.g., ZnO) with low electrical conductivity and reversibility [54]. To further improve the cycling stability of Zn-based batteries, it is essential to design the nanostructured Zn electrodes with high reversibility instead of using a Zn foil [28].

3.4. Performance of the Zn-air battery

Before assembling in Zn-air batteries, we coated a PTFE layer on the Co_3O_4/Ni foam electrode to build the triple-phase boundaries that facilitate the gaseous oxygen transport [53]. For the discharge polarization (Fig. 5a), a maximum power density of 35.7 mW cm^{-2} is delivered when the current density reaches 68 mA cm^{-2}. Compared to some reported power densities of the electrodes made by the combination of the catalyst, carbon additives, and polymer binders [54], this low value may be caused by the poor conductivity due to the absence of carbon and the poor-established triple-phase boundaries [20]. Similarly, a Zn-air battery with an integrated electrode made of Co_3O_4 nanowire array on stainless steel mesh was reported to deliver a maximum power density of ~40 mW cm^{-2} [37]. Even so, the obtained power density is higher than those of batteries with some newly-developed catalysts, such as Co_3O_4 nanoparticle-decorated carbon nanofiber mat (~28 mW cm^{-2}) [30], Co_3O_4 decorated N-doped Vulcan carbon (33 mW cm^{-2}) [55], core–shell-structured Co@Co3O4 nanoparticles packaged into N-doped carbon polyhedral (~32 mW cm^{-2}) [56], and $Co(OH)_2$ compounding with N-doped graphene oxide (~35 mW cm^{-2}) [57]. The galvanostatic discharge performance is measured using low and high current densities of 5 and 20 mA cm^{-2}, respectively. As shown in Fig. 5b, the voltage plateaus at 1.16 and 1.0 V are presented, respectively, consistent with the polarization curves. In addition, the specific capacities based on the consumed zinc are 771 and 719 mA h g_{Zn}^{-1}, respectively, approximate to the theoretical value of Zn (820 mAh

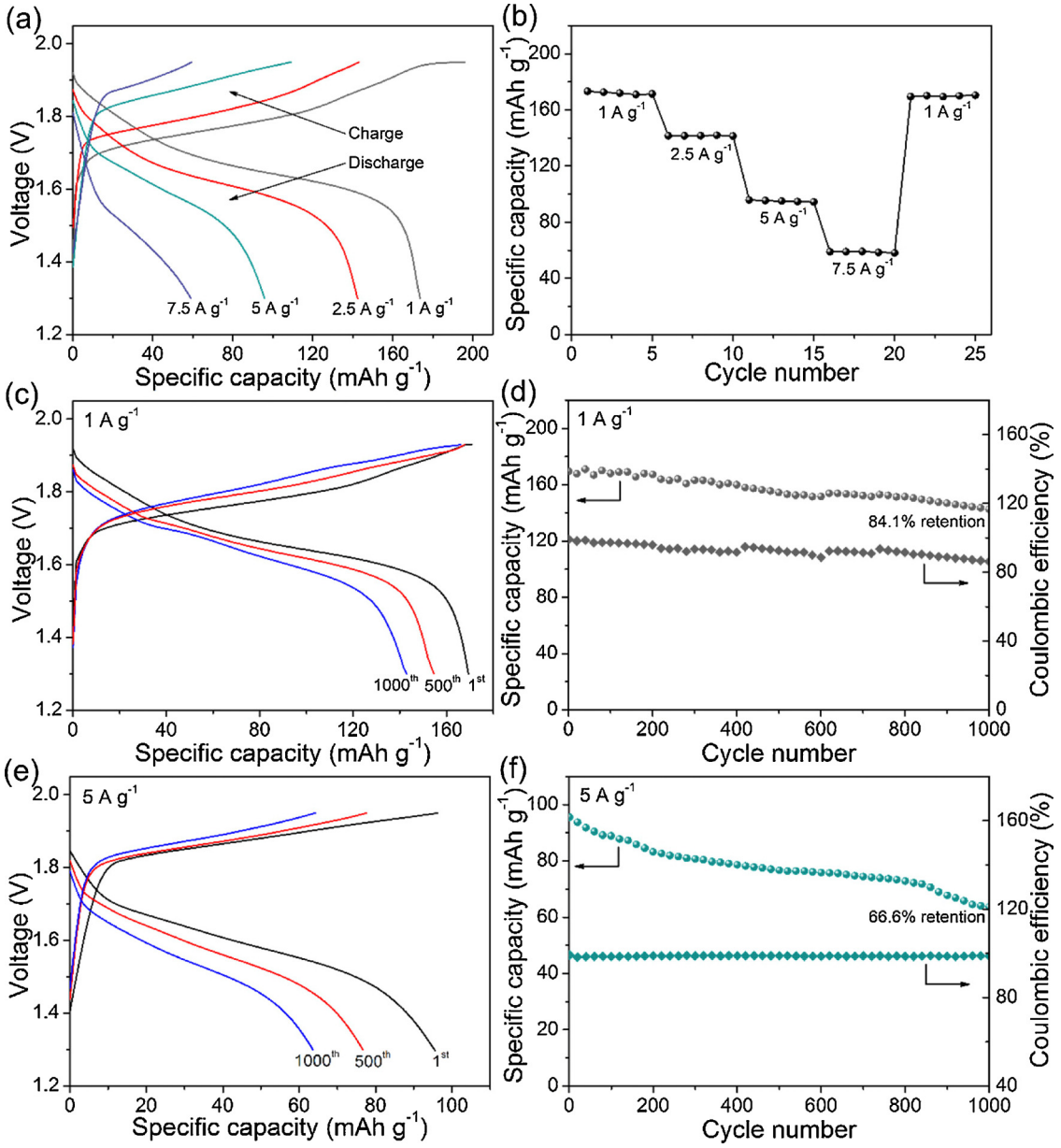

Fig. 4. Electrochemical performance of the Zn-Co_3O_4 battery. (a) Charge and discharge voltage curves between 1.30 and 1.95 V. (b) Summary of discharge capacities at various current densities. (c and e) Charge and discharge curves of the 1st, 500th, and 1000th cycle at (c) 1 A g^{-1} between 1.30 and 1.93 V and (e) 5 A g^{-1} between 1.30 and 1.95 V (d and f) Capacity retention ratio and coulombic efficiency during the cycling test at (d) 1 A g^{-1} and (f) 5 A g^{-1}.

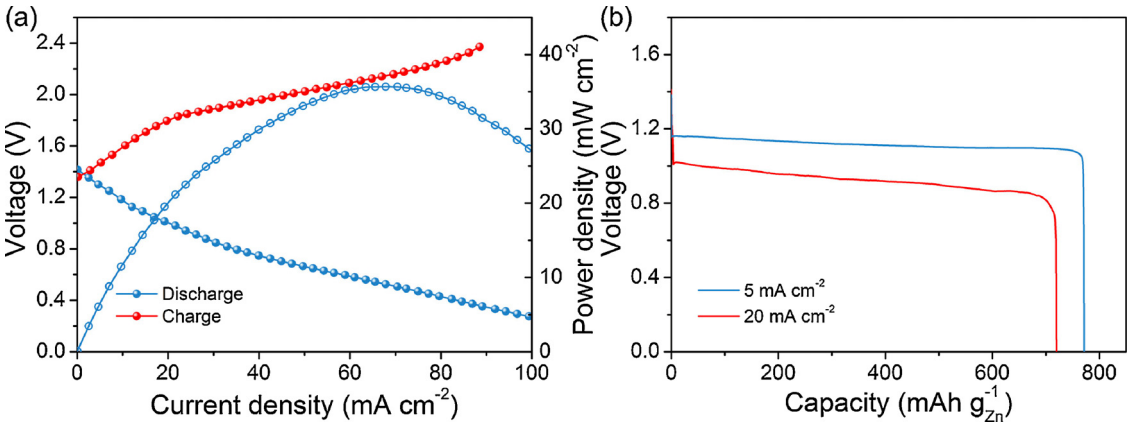

Fig. 5. Electrochemical performance of a Zn-air battery with the Co_3O_4/Ni foam electrode. (a) Polarization curves and the corresponding power density. (b) Discharge voltage profiles at constant current densities of 5 and 20 mA cm^{-2}.

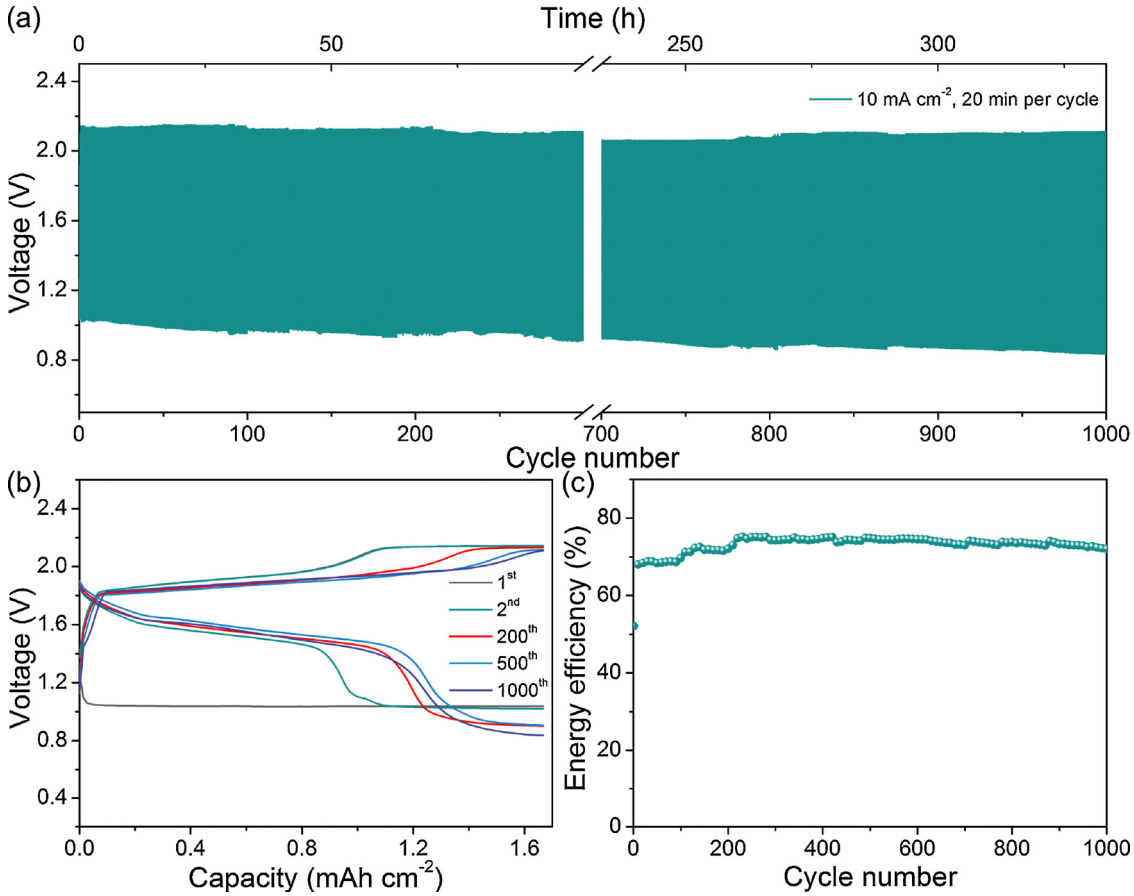

Fig. 6. Long-term cycling stability of a Zn-air battery with the Co_3O_4/Ni foam electrode. (a) Voltage profiles at 10 mA cm^{-2} (20 min per cycle). (b) Voltage profiles of the 1st, 2nd, 200th, 500th, and 1000th cycle. (c) Energy efficiency throughout the cycling test.

g_{Zn}^{-1}). For the charge process, even the current density increases to 88 mA cm^{-2}, the voltage only researches 2.37 V. This good charge performance may come from the hierarchical electrode structure, which not only favors the rapid charge transfer during the catalytic reactions, but also facilitates the release of produced oxygen.

The stability of the Co_3O_4/Ni foam electrode in a Zn-air battery was further evaluated by pulse discharge-charge tests using a current density of 10 mA cm^{-2} with a fixed capacity of 1.67 mA cm^{-2} (20 min per cycle). As clearly illustrated in Fig. 6b, a flat plateau at the voltage of 1.06 V is shown in the first discharge process, indicating the ORR process. In the following charge process, two voltage plateaus are observed, which correspond to the evolution of Co_3O_4 and the OER. Consequently, two voltage regions are delivered in the following discharge process: the first one at the voltage of ~1.6 V refers to the reduction of Co_3O_4 as demonstrated in the Zn-Co_3O_4 battery, while the second plateau at 1.05 V is related to the ORR process in the Zn-air battery. Hence, the discharge and charge behaviors of both Zn-Co_3O_4 and zinc-air batteries coexist, similar to the reported hybrid Zn battery using the $NiCo_2O_4$ nanowire electrode [53]. The two-step voltage profile was retained starting from the second cycle. It is found that the capacity of the Zn-Co_3O_4 reaction over the first 200 cycles gradually increased, and became stable afterward (Fig. S7). The similar phenomenon has been reported in hybrid Zn batteries, which may be caused by the increase of the electroactive sites accessible by the electrolyte [53]. Impressively, the battery can be cycled for over 1000 times (333 h) with quite stable charge voltages and little-decreased discharge voltages (Fig. 6a). The degradation may be caused by the following reasons: First, the binder (PTFE) may be detached from the air electrode, resulting in the decrease of triple-phase boundaries, and thus affect the gaseous oxygen transport. Second, carbon dioxide in the air can enter the battery, and water can evaporate during the long-term cycling test, both of which gradually affect the ionic conductivity of the electrolyte [18]. Third, the formation of dendrite and passivation layers of the Zn electrode affects the reversibility, increasing the polarization. Hence, the developments of stable electrodes to maintain triple-phase boundaries [20], functional membranes that prevent CO_2 penetration and water solvent evaporation [2], and stable Zn electrodes with high reversibility are essential to the long-term stability. Attributed to the hybrid behaviours including the transition between metal oxide and hydroxide and the ORR and OER, when compared with conventional Zn-air batteries that only include the ORR and OER, the energy consumed on charge is reduced while the energy delivered on discharge is increased, leading to an improved energy efficiency of around 70% (Fig. 6c) [8]. It is worth noting that although the Zn-Co_3O_4 reaction only contributes to a limited capacity under the condition of sufficient Zn at a full discharge depth, a fixed capacity is generally used for charge-discharge cycles to avoid the failure of reaction boundaries in rechargeable metal-air batteries [58,59]. At a given depth of discharge, the percentage of the Zn-Co_3O_4 reaction can account for a large percentage of the cycling capacity and greatly affect the discharge and charge voltages. Thus, in practical applications, the depth of discharge during cycling and the amount of Co_3O_4 should be carefully designed to achieve the high energy efficiency.

Taking advantage of the rapid redox reactions of Co_3O_4 in the Zn-Co_3O_4 reaction region, the charging time may be greatly shortened. To this end, the high-rate capability of this Co_3O_4/Ni foam electrode was further evaluated through cycling in a fixed capacity at different charge current densities (2 to 16 mA cm^{-2}) but the same discharge current density (2 mA cm^{-2}). From the results in Fig. S8a, the charge voltages gradually increase when increasing the current density from 2 to 16 mA

cm^{-2}. Even so, the discharge voltage curve and the capacity of the Zn-Co_3O_4 reaction are virtually unchanged (Fig. S8b). This allows reducing the charging time while maintaining both the discharge voltage and the capacity, which is significant for the applications of "fast charging" in electric vehicles and electronic devices [60].

4. Conclusions

In this work, we have developed an electrode composed of Co_3O_4 nanowire-assembled clusters on nickel foam using a hydrothermal method and a calcination process. The SEM and TEM analyses reveal that porous Co_3O_4 nanowires are directly coupled to the underlying nickel foam to form clusters, greatly reducing the resistance in the interface and improving the electrical conductivity. Besides, the porous nanoarchitecture offers large surface areas and pore volumes, which are beneficial for electrochemical reactions and species transport. Moreover, the assembled clusters are favorable for the structural stability. These features are essential for the high activity toward both ORR and OER and the large specific capacitance, demonstrating the potential for rechargeable zinc batteries. When applied this electrode in a Zn-Co_3O_4 battery, it delivers an energy density of 239 Wh kg^{-1} on the basis of Co_3O_4 loading and the theoretical capacity of zinc, and the capacity retention reaches 84.1% after 1000 cycles. Even at a much higher current density of 5 A g^{-1}, the capacity retention still reaches 66.6% after 1000 cycles. To further extend its application, a Zn-air battery with this electrode presents a power density up to 35.7 mW cm^{-2}, a gravimetric capacity of 771 mAh $g_{Zn}{}^{-1}$, and excellent cycling stability for over 1000 cycles (over 333 h) at 10 mA cm^{-2} with a fixed capacity of 1.67 mA cm^{-2} while maintaining the energy efficiency of 70%. Hence, the nickel foam coated with Co_3O_4 nanowire-assembled clusters is a promising positive electrode for rechargeable zinc batteries with high energy density, energy efficiency, and cycling stability. It is worth noting that the present study focused on the positive electrode, while the negative electrode (zinc) may suffer from dendrite and passivation during the long-term cycling, which will decrease the electrochemical performance and cause the safety issues [54]. Therefore, besides the development and optimization of the positive electrode, developing a highly reversible Zn electrode is crucial for the stability of rechargeable Zn-based batteries [61,62], which will be our continuous research topics.

Acknowledgments

P. Tan thanks the funding support from CAS Pioneer Hundred Talents Program. M. Ni thanks the funding support from The Hong Kong Polytechnic University (G-YBJN and G-YW2D), a fund from RISUD (1-ZVEA), and a grant (Project Number: PolyU 152214/17E) from Research Grant Council, University Grants Committee, Hong Kong SAR.

Appendix A. Supplementary data

Supplementary material related to this article can be found, in the online version, at doi:https://doi.org/10.1016/j.apcatb.2018.09.017.

References

[1] B. Dunn, H. Kamath, J.-M. Tarascon, Electrical Energy Storage for the Grid: A Battery of Choices, Science 334 (2011) 928–935.
[2] P. Tan, B. Chen, H. Xu, H. Zhang, W. Cai, M. Ni, M. Liu, Z. Shao, Flexible Zn– and Li–air batteries: recent advances, challenges, and future perspectives, Energy Environ. Sci. 10 (2017) 2056–2080.
[3] Z.-L. Wang, D. Xu, J.-J. Xu, X.-B. Zhang, Oxygen electrocatalysts in metal-air batteries: from aqueous to nonaqueous electrolytes, Chem. Soc. Rev. 43 (2014) 7746–7786.
[4] E.J. Cairns, P. Albertus, Batteries for electric and hybrid-electric vehicles, Annu. Rev. Chem. Biomol. Eng. 1 (2010) 299–320.
[5] R. Schmuch, R. Wagner, G. Hörpel, T. Placke, M. Winter, Performance and cost of materials for lithium-based rechargeable automotive batteries, Nat. Energy. 3 (2018) 267–278.
[6] E. Hu, X. Yang, Rejuvenating zinc batteries, Nat. Mater. 17 (2018) 480–481.
[7] Z.P. Cano, D. Banham, S. Ye, A. Hintennach, J. Lu, M. Fowler, Z. Chen, Batteries and fuel cells for emerging electric vehicle markets, Nat. Energy. 3 (2018) 279–289.
[8] Y. Li, H. Dai, Recent advances in zinc–air batteries, Chem. Soc. Rev. 43 (2014) 5257–5275.
[9] H. Pan, Y. Shao, P. Yan, Y. Cheng, K.S. Han, Z. Nie, C. Wang, J. Yang, X. Li, P. Bhattacharya, K.T. Mueller, J. Liu, Reversible aqueous zinc/manganese oxide energy storage from conversion reactions, Nat. Energy. 1 (2016) 16039.
[10] W. Sun, F. Wang, S. Hou, C. Yang, X. Fan, Z. Ma, T. Gao, F. Han, R. Hu, M. Zhu, C. Wang, Zn/MnO_2 Battery Chemistry With H^+ and Zn^{2+}Coinsertion, J. Am. Chem. Soc. 139 (2017) 9775–9778.
[11] M. Gong, Y. Li, H. Zhang, B. Zhang, W. Zhou, J. Feng, H. Wang, Y. Liang, Z. Fan, J. Liu, H. Dai, Ultrafast high-capacity NiZn battery with NiAlCo-layered double hydroxide, Energy Environ. Sci. 7 (2014) 2025–2032.
[12] Y.P. Wu, X. Wang, M. Li, Y. Wang, B. Chen, Y. Zhu, A Zn-NiO rechargeable battery with long lifespan and high energy density, J. Mater. Chem. A 3 (2015) 8280–8283.
[13] D. Ozgit, P. Hiralal, G.A.J. Amaratunga, Improving performance and cyclability of zinc-silver oxide batteries by using graphene as a two dimensional conductive additive, ACS Appl. Mater. Interfaces 6 (2014) 20752–20757.
[14] R. Kumar, J. Shin, L. Yin, J.-M. You, Y.S. Meng, J. Wang, All-Printed, Stretchable Zn-Ag_2O Rechargeable Battery via Hyperelastic Binder for Self-Powering Wearable Electronics, Adv. Energy Mater. 7 (2017) 1602096.
[15] A.M. Zamarayeva, A.E. Ostfeld, M. Wang, J.K. Duey, I. Deckman, B.P. Lechêne, G. Davies, D.A. Steingart, A.C. Arias, Flexible and stretchable power sources for wearable electronics, Sci. Adv. 3 (2017) e1602051.
[16] F.R. McLarnon, E.J. Cairns, The Secondary Alkaline Zinc Electrode, J. Electrochem. Soc. 138 (1991) 645–656.
[17] J. Shin, J.-M. You, J.Z. Lee, R. Kumar, L. Yin, J. Wang, Y. Shirley Meng, Deposition of ZnO on bismuth species towards a rechargeable Zn-based aqueous battery, Phys. Chem. Chem. Phys. 18 (2016) 26376–26382.
[18] J.-S. Lee, S.T. Kim, R. Cao, N.-S. Choi, M. Liu, K.T. Lee, J. Cho, Metal-air batteries with high energy density: Li-Air versus Zn-Air, Adv. Energy Mater. 1 (2011) 34–50.
[19] J. Liu, L. Jiang, Q. Tang, E. Wang, L. Qi, S. Wang, G. Sun, Amide-functionalized carbon supports for cobalt oxide toward oxygen reduction reaction in Zn-air battery, Appl. Catal. B Environ. 148–149 (2014) 212–220.
[20] F. Cheng, J. Chen, Metal–air batteries: from oxygen reduction electrochemistry to cathode catalysts, Chem. Soc. Rev. 41 (2012) 2172–2192.
[21] P. Tan, H.R. Jiang, X.B. Zhu, L. An, C.Y. Jung, M.C. Wu, L. Shi, W. Shyy, T.S. Zhao, Advances and challenges in lithium-air batteries, Appl. Energy 204 (2017) 780–806.
[22] D.U. Lee, P. Xu, Z.P. Cano, A.G. Kashkooli, M.G. Park, Z. Chen, Recent progress and perspectives on bi-functional oxygen electrocatalysts for advanced rechargeable metal–air batteries, J. Mater. Chem. A 4 (2016) 7107–7134.
[23] V. Caramia, B. Bozzini, Materials science aspects of zinc–air batteries: a review, Mater. Renew. Sustain. Energy 3 (2014) 28.
[24] V. Neburchilov, H. Wang, J.J. Martin, W. Qu, A review on air cathodes for zinc–air fuel cells, J. Power Sources 195 (2010) 1271–1291.
[25] J.E. Park, M.-J. Kim, M.S. Lim, S.Y. Kang, J.K. Kim, S.-H. Oh, M. Her, Y.-H. Cho, Y.-E. Sung, Graphitic carbon nitride-carbon nanofiber as oxygen catalyst in anion-exchange membrane water electrolyzer and rechargeable metal–air cells, Appl. Catal. B Environ. 237 (2018) 140–148.
[26] M.H. Seo, M.G. Park, D.U. Lee, X. Wang, W. Ahn, S.H. Noh, S.M. Choi, Z.P. Cano, B. Han, Z. Chen, Bifunctionally Active and Durable Hierarchically Porous Transition Metal-based Hybrid Electrocatalyst for Rechargeable Metal-Air Batteries, Appl. Catal. B Environ. 239 (2018) 677–687.
[27] A. Arul, H. Pak, K.U. Moon, M. Christy, M.Y. Oh, K.S. Nahm, Metallomacrocyclic–carbon complex: A study of bifunctional electrocatalytic activity for oxygen reduction and oxygen evolution reactions and their lithium-oxygen battery applications, Appl. Catal. B Environ. 220 (2018) 488–496.
[28] X. Wang, F. Wang, L. Wang, M. Li, Y. Wang, B. Chen, Y. Zhu, L. Fu, L. Zha, L. Zhang, Y. Wu, W. Huang, An Aqueous Rechargeable Zn//Co_3O_4Battery with High Energy Density and Good Cycling Behavior, Adv. Mater. 28 (2016) 4904–4911.
[29] D.U. Lee, M.G. Park, H.W. Park, M.H. Seo, X. Wang, Z. Chen, Highly Active and Durable Nanocrystal-Decorated Bifunctional Electrocatalyst for Rechargeable Zinc-Air Batteries, ChemSusChem 8 (2015) 3129–3138.
[30] B. Li, X. Ge, F.W.T. Goh, T.S.A. Hor, D. Geng, G. Du, Z. Liu, J. Zhang, X. Liu, Y. Zong, Co_3O_4 nanoparticles decorated carbon nanofiber mat as binder-free air-cathode for high performance rechargeable zinc-air batteries, Nanoscale 7 (2015) 1830–1838.
[31] P. Tan, B. Chen, H. Xu, W. Cai, W. He, M. Liu, Z. Shao, M. Ni, Co_3O_4 Nanosheets as Active Material for Hybrid Zn Batteries, Small 14 (2018) 1800225.
[32] D. Kong, J. Luo, Y. Wang, W. Ren, T. Yu, Y. Luo, Y. Yang, C. Cheng, Three-Dimensional Co_3O_4@MnO_2Hierarchical Nanoneedle Arrays: Morphology Control and Electrochemical Energy Storage, Adv. Funct. Mater. 24 (2014) 3815–3826.
[33] R.R. Salunkhe, J. Lin, V. Malgras, S.X. Dou, J.H. Kim, Y. Yamauchi, Large-scale synthesis of coaxial carbon nanotube/$Ni(OH)_2$ composites for asymmetric supercapacitor application, Nano Energy 11 (2015) 211–218.
[34] Z. Zhu, J. Ping, X. Huang, J. Hu, Q. Chen, X. Ji, C.E. Banks, Hexagonal nickel oxide nanoplate-based electrochemical supercapacitor, J. Mater. Sci. 47 (2012) 503–507.
[35] F. Cheng, J. Chen, Lithium-air batteries: something from nothing, Nat. Chem. 4 (2012) 962–963.
[36] Y. Sun, J. Liu, J. Song, S. Huang, N. Yang, J. Zhang, Y. Sun, Y. Zhu, Exploring the Effect of Co_3O_4Nanocatalysts with Different Dimensional Architectures on Methane Combustion, ChemCatChem 8 (2016) 540–545.

[37] D.U. Lee, J.-Y. Choi, K. Feng, H.W. Park, Z. Chen, Advanced Extremely Durable 3D Bifunctional Air Electrodes for Rechargeable Zinc-Air Batteries, Adv. Energy Mater. 4 (2014) 1301389.
[38] P. Tan, M. Liu, Z. Shao, M. Ni, Recent Advances in Perovskite Oxides as Electrode Materials for Nonaqueous Lithium-Oxygen Batteries, Adv. Energy Mater. 7 (2017) 1602674.
[39] I.G. Casella, M. Gatta, Study of the electrochemical deposition and properties of cobalt oxide species in citrate alkaline solutions, J. Electroanal. Chem. 534 (2002) 31–38.
[40] P. Nkeng, Characterization of spinel-type cobalt and nickel oxide thin films by X-Ray near grazing diffraction, transmission and reflectance spectroscopies, and cyclic voltammetry, J. Electrochem. Soc. 142 (1995) 1777–1783.
[41] P. Bhojane, L. Sinha, R.S. Devan, P.M. Shirage, Mesoporous layered hexagonal platelets of Co_3O_4 nanoparticles with (111) facets for battery applications: high performance and ultra-high rate capability, Nanoscale. 10 (2018) 1779–1787.
[42] E.B. Castro, C.A. Gervasi, J.R. Vilche, Oxygen evolution on electrodeposited cobalt oxides, J. Appl. Electrochem. 28 (1998) 835–841.
[43] S.K. Meher, G.R. Rao, Effect of microwave on the nanowire morphology, optical, magnetic, and pseudocapacitance behavior of Co_3O_4, J. Phys. Chem. C 115 (2011) 25543–25556.
[44] A. Qaseem, F. Chen, C. Qiu, A. Mahmoudi, X. Wu, X. Wang, R.L. Johnston, Reduced graphene oxide decorated with manganese cobalt oxide as multifunctional material for mechanically rechargeable and hybrid zinc-air batteries, Part. Part. Syst. Charact. 34 (2017) 1700097.
[45] S. Venkatraman, Y. Shin, A. Manthiram, Phase relationships and structural and chemical stabilities of charged $Li_{1-x}CoO_{2-\delta}$ and $Li_{1-x}Ni_{0.85}Co_{0.15}O_{2-\delta}$ cathodes, Electrochem. Solid-State Lett. 6 (2003) A9–A12.
[46] T. Motohashi, Y. Katsumata, T. Ono, R. Kanno, M. Karppinen, H. Yamauchi, Synthesis and properties of CoO_2, the $x=0$ end member of the Li_xCoO_2 and Na_xCoO_2 systems, Chem. Mater. 19 (2007) 5063–5066.
[47] J. Liu, C. Guan, C. Zhou, Z. Fan, Q. Ke, G. Zhang, C. Liu, J. Wang, A flexible quasi-solid-State nickel–Zinc battery with high energy and power densities based on 3D electrode design, Adv. Mater. 28 (2016) 8732–8739.
[48] B. Zhang, Y. Liu, X. Wu, Y. Yang, Z. Chang, Z. Wen, Y. Wu, An aqueous rechargeable battery based on zinc anode and $Na_{0.9}MnO_2$, Chem. Commun. 50 (2014) 1209–1211.
[49] F. Wang, Y. Liu, X. Wang, Z. Chang, Y. Wu, R. Holze, Aqueous rechargeable battery based on zinc and a composite of $LiNi_{1/3}Co_{1/3}Mn_{1/3}O_2$, ChemElectroChem 2 (2015) 1024–1030.
[50] F. Wang, F. Yu, X. Wang, Z. Chang, L. Fu, Y. Zhu, Z. Wen, Y. Wu, W. Huang, Aqueous rechargeable Zinc/Aluminum ion battery with good cycling performance, ACS Appl. Mater. Interfaces 8 (2016) 9022–9029.
[51] M. Song, H. Tan, D. Chao, H.J. Fan, Recent advances in Zn-Ion batteries, Adv. Funct. Mater. (2018) 1802564.
[52] X. Wang, M. Li, Z. Chang, Y. Yang, Y. Wu, X. Liu, Co_3O_4@MWCNT nanocable as cathode with superior electrochemical performance for supercapacitors, ACS Appl. Mater. Interfaces 7 (2015) 2280–2285.
[53] B. Li, J. Quan, A. Loh, J. Chai, Y. Chen, C. Tan, X. Ge, T.S.A. Hor, Z. Liu, H. Zhang, Y. Zong, A robust hybrid Zn-battery with ultralong cycle life, Nano Lett. 17 (2017) 156–163.
[54] J. Fu, Z.P. Cano, M.G. Park, A. Yu, M. Fowler, Z. Chen, Electrically Rechargeable Zinc-Air Batteries: Progress, Challenges, and Perspectives, Adv. Mater. 29 (2017) 1604685.
[55] T. An, X. Ge, T.S.A. Hor, F.W.T. Goh, D. Geng, G. Du, Y. Zhan, Z. Liu, Y. Zong, Co_3O_4 nanoparticles grown on N-doped Vulcan carbon as a scalable bifunctional electro-catalyst for rechargeable zinc–air batteries, RSC Adv. 5 (2015) 75773–75780.
[56] Z. Guo, F. Wang, Y. Xia, J. Li, A.G. Tamirat, Y. Liu, L. Wang, Y. Wang, Y.-Y. Xia, In situ encapsulation of core–shell-structured Co@Co_3O_4 into nitrogen-doped carbon polyhedra as a bifunctional catalyst for rechargeable Zn–air batteries, J. Mater. Chem. A 6 (2018) 1443–1453.
[57] Y. Zhan, G. Du, S. Yang, C. Xu, M. Lu, Z. Liu, J.Y. Lee, Development of Cobalt Hydroxide as a Bifunctional Catalyst for Oxygen Electrocatalysis in Alkaline Solution, ACS Appl. Mater. Interfaces 7 (2015) 12930–12936.
[58] J. Lu, L. Li, J.B. Park, Y.K. Sun, F. Wu, K. Amine, Aprotic and aqueous Li-O_2 batteries, Chem. Rev. 114 (2014) 5611–5640.
[59] Y. Li, J. Lu, Metal–Air Batteries: Will They Be the Future Electrochemical Energy Storage Device of Choice? ACS Energy Lett. 2 (2017) 1370–1377.
[60] C. Sun, J. Liu, Y. Gong, D.P. Wilkinson, J. Zhang, Recent advances in all-solid-state rechargeable lithium batteries, Nano Energy 33 (2017) 363–386.
[61] J.F. Parker, C.N. Chervin, I.R. Pala, M. Machler, M.F. Burz, J.W. Long, D.R. Rolison, Rechargeable nickel–3D zinc batteries: an energy-dense, safer alternative to li-thium-ion, Science 356 (2017) 415–418.
[62] F. Wang, O. Borodin, T. Gao, X. Fan, W. Sun, F. Han, A. Faraone, J.A. Dura, K. Xu, C. Wang, Highly reversible zinc metal anode for aqueous batteries, Nat. Mater. 17 (2018) 543–549.